

1-1-2007

Motion-Sensitive 3-D Optical Coherence Microscope Operating at 1300 nm for the Visualization of Early Frog Development

Barbara M. Hoeling
California State Polytechnic University - Pomona

Stephanie S. Feldman

Daniel T. Streng

Aaron Bernard

Emily R. Hogan

See next page for additional authors

Recommended Citation

Hoeling, B.M., S.S. Feldman, D.T. Streng, A. Bernard, E.R. Hogan, D.C. Petersen, S.E. Fraser, Y. Kee, J.M. Tyszka, and R.C. Haskell. Barbara M. Hoeling, Stephanie S. Feldman, Daniel T. Streng, Aaron Bernard, Emily R. Hogan, Daniel C. Petersen, Scott E. Fraser, Yun Kee, J. Michael Tyszka and Richard C. Haskell, "Motion-sensitive 3-D optical coherence microscope operating at 1300 nm for the visualization of early frog development", Proc. SPIE 6429, 64292T (2007); <http://dx.doi.org/10.1117/12.701420>

This Conference Proceeding is brought to you for free and open access by the HMC Faculty Scholarship at Scholarship @ Claremont. It has been accepted for inclusion in All HMC Faculty Publications and Research by an authorized administrator of Scholarship @ Claremont. For more information, please contact scholarship@cuc.claremont.edu.

Authors

Barbara M. Hoeling, Stephanie S. Feldman, Daniel T. Strenge, Aaron Bernard, Emily R. Hogan, Daniel C. Petersen, Scott E. Fraser, Yun Kee, J. Michael Tyszka, and Richard C. Haskell

Motion-Sensitive 3-D Optical Coherence Microscope Operating at 1300 nm for the Visualization of Early Frog Development

Barbara M. Hoeling¹, Stephanie S. Feldman², Daniel T. Streng²,
Aaron Bernard², Emily R. Hogan², Daniel C. Petersen², Scott E. Fraser³,
Yun Kee³, J. Michael Tyszka³, Richard C. Haskell²

¹Department of Physics and Astronomy, Pomona College, Claremont, CA, USA

²Department of Physics, Harvey Mudd College, Claremont, CA, USA

³Biological Imaging Center, California Institute of Technology, Pasadena, CA, USA

ABSTRACT

We present 3-dimensional volume-rendered *in vivo* images of developing embryos of the African clawed frog *Xenopus laevis* taken with our new *en-face*-scanning, focus-tracking OCM system at 1300 nm wavelength. Compared to our older instrument which operates at 850 nm, we measure a decrease in the attenuation coefficient by 33%, leading to a substantial improvement in depth penetration. Both instruments have motion-sensitivity capability. By evaluating the fast Fourier transform of the fringe signal, we can produce simultaneously images displaying the fringe amplitude of the backscattered light and images showing the random Brownian motion of the scatterers. We present time-lapse movies of frog gastrulation, an early event during vertebrate embryonic development in which cell movements result in the formation of three distinct layers that later give rise to the major organ systems. We show that the motion-sensitive images reveal features of the different tissue types that are not discernible in the fringe amplitude images. In particular, we observe strong diffusive motion in the vegetal (bottom) part of the frog embryo which we attribute to the Brownian motion of the yolk platelets in the endoderm.

1. INTRODUCTION

Optical Coherence Microscopy (OCM) is a non-invasive biomedical imaging technique similar to Optical Coherence Tomography (OCT) [1]. Unlike OCT, which performs depth scans into highly scattering biological tissue and is used, for example, in endoscopic probes for optical biopsies, OCM delivers 3-dimensional images by performing consecutive *en-face* plane scans at increasing tissue depths. One of its main areas of application is developmental biology, e.g., the visualization of developing vertebrate embryos.

The process of gastrulation, the first major morphological event in vertebrate development, is of particular interest in developmental biology. It involves the migration and differentiation of cells into three tissue layers: the ectoderm (future skin and nervous system), the mesoderm (future circulatory system and muscle tissue), and the endoderm (future digestive tract lining and various internal organs). Optical microscopy of the deeper tissues is difficult to perform on the developing embryos. Many animal model systems of interest in developmental biology have opaque embryos and tissues and may require the temporal and spatial imaging of those live embryos to understand their development.

With our OCM instrument, we are able to image frog embryos non-invasively and *in vivo*, thus following the development of a single frog embryo. We are simultaneously taking two types of images, one that displays the fringe amplitude, i.e., the intensity of the backscattered light, and one that visualizes the diffusive motion of the scatterers in the different tissue types. The two kinds of images reveal additional and complementary information about the embryonic tissue and the frog development.

2. EXPERIMENTAL METHODS

2.1 Characteristics of the new 1300nm OCM instrument

The design of our new 1300 nm OCM instrument is similar to the 850 nm OCM that has been described previously in three publications [2-4]. Here we will summarize the most important performance specifications and improvements over the old instrument.

With a central wavelength of 1303 nm and a spectral bandwidth (FWHM) of 46.5 nm, the new OCM achieves a depth resolution of 16 μm in air, or 11-12 μm in water or tissue. The lateral resolution of 5 μm corresponds to the waist diameter of the focused beam. Both resolutions are about the same for the two instruments, and comparable to the typical size of cells in developing frog embryos, so individual cells can sometimes be resolved. Two galvoscaning mirrors perform an *en face* scan of the tissue, then the sample head with the focusing lens is stepped down in the z-direction for imaging the next x-y plane deeper into the tissue while the reference mirror is translated to keep the equal path length position coincident with the focused waist of the beam ("focus-tracking"). Figure 1 shows a schematic of the instrument.

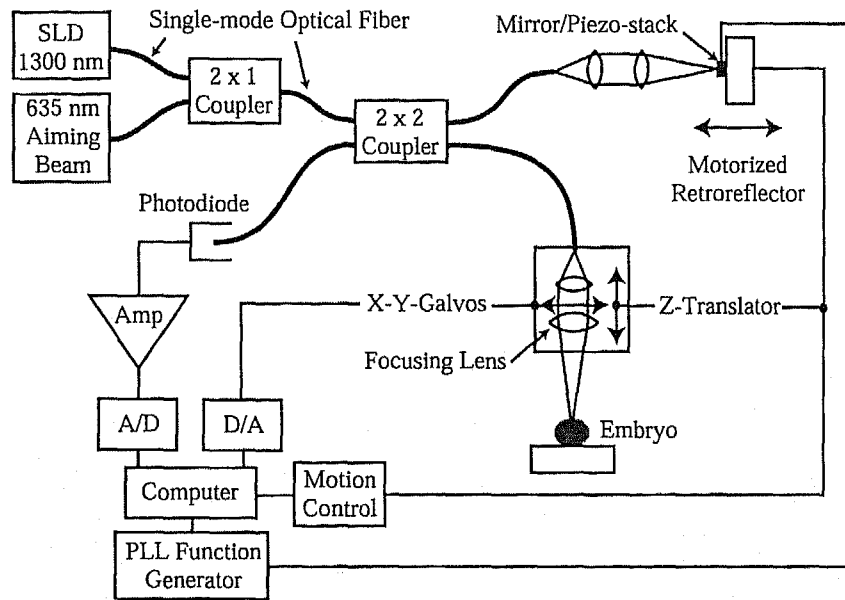


Fig. 1: Schematic of the 1300 nm OCM instrument.

The scattering and absorption within a sample attenuate the strength of the fringe signal as the OCM scans deeper into the sample. The signal decay depends on the specific optical properties of the sample at the wavelength of the incident light and can be modeled by an exponential function:

$$\text{Fringe amplitude signal} \propto e^{-\mu * \text{depth}} \quad \text{Eq.(1)}$$

Here, μ is the total attenuation coefficient, which is a measure of how quickly the signal decays in a given sample.

In order to determine the attenuation coefficients for the light sources of both the 850 nm and 1300 nm OCMs, we used fringe amplitude data from various images obtained with the two instruments. We plotted the average fringe amplitude of each plane versus the depth of the plane. Figure 2 shows a graph of a sample (cropped) image with the exponential fit that yields the attenuation coefficient. This analysis is straightforward because of our focus-tracking system that keeps the beam waist coincident with the coherence volume. Our final attenuation coefficients were determined as the means of the values of about a dozen images for each instrument, with standard error for uncertainty. The attenuation coefficient in frog embryo tissue for 1300 nm light was measured to be $(20 \pm 1) \text{ mm}^{-1}$, a decrease by 33% compared to $(30.0 \pm 0.6) \text{ mm}^{-1}$ for 850 nm light.

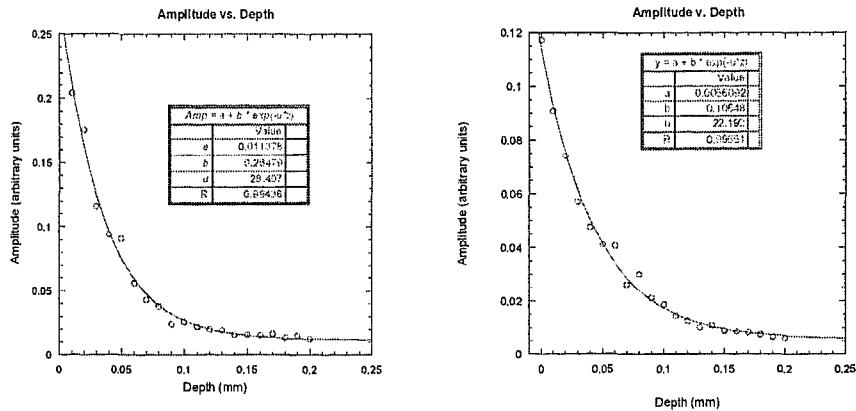


Fig. 2: Plane average of fringe amplitude vs. depth of plane. The left graph displays data of an image taken with the 850 nm instrument. The attenuation coefficient for this particular image, as determined from the exponential fit, is 28.4 mm^{-1} . The graph on the right shows data of an image taken with the 1300 nm instrument, yielding an attenuation coefficient of 22.2 mm^{-1} .

Fig. 3 shows the substantial improvement in penetration depth of the 1300 nm instrument.

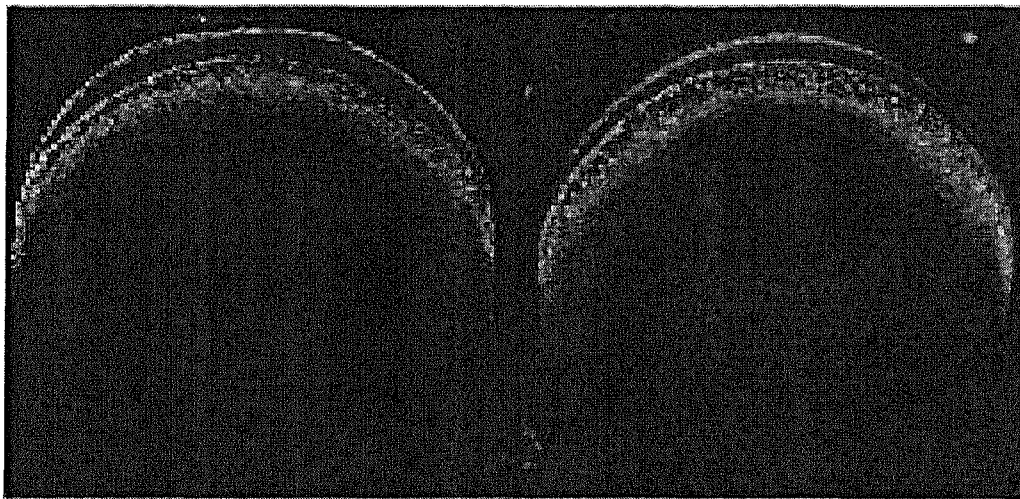


Fig. 3: Both of the above fringe amplitude images were taken at a similar stage in embryonic development. Red voxels indicate highly scattering, blue voxels weakly scattering tissue. The left image was taken with the 850 nm OCM, the right image with the 1300 nm OCM. Each embryo is approximately 1.5 mm in diameter. The depth penetration is clearly improved by about one third with the 1300 nm OCM.[5]

2.2 Description of Motion Sensitivity

The interference term (the fringe signal) of the OCM is given by:

$$Signal = 2\sqrt{P_{ref}P_{samp}} \cos\left[\frac{4\pi d_0}{\lambda} \sin \omega_{piezo} t + \frac{4\pi n}{\lambda} z_{scat}(t) + \Psi(t)\right] \quad Eq.(2)$$

The first term in the phase of Eq. (2) is the one that generates the “fringe signal”. It is due to the motion of the reference mirror which is glued to an oscillating piezo stack. The piezo is driven sinusoidally at its resonance frequency of $\omega_{piezo} = 2\pi \cdot 85.85 \cdot 10^3$ rad/s, and with a peak-to-peak amplitude of $2d_0 = 0.600\lambda$ or $\alpha \equiv 4\pi d_0 / \lambda = 3.77$, such that the sum of the powers in the 2nd and 3rd harmonics ($2\omega_{piezo}$ and $3\omega_{piezo}$) is independent of any slow phase drift [4]. The second term describes the (slower) phase variation due to the motion of the scatterer along the direction of the beam (the z-axis). Here, n is the refractive index of the medium in which the scatterer is moving. The last term $\Psi(t)$ is the slowest varying one, the thermal phase drift (0.1 to 1 Hz), which can be neglected in the calculation of the diffusive motion.

The OCM software performs a fast Fourier transform (FFT) on the digitally sampled data from each volume element and uses the Fourier coefficients in the 2nd and 3rd harmonics to calculate the fringe amplitude and phase $\phi(t)$ associated with each voxel in the following way:

$$Fringe \text{ Amplitude} = \sqrt{P_{2\omega} + P_{3\omega}}, \quad Eq.(3)$$

where $P_{2\omega}$ and $P_{3\omega}$ are the powers in the 2nd and 3rd harmonics, respectively, and

$$\phi(t) = \arctan\left(\frac{-b_3}{a_2}\right), \quad Eq.(4)$$

where b_3 is the Fourier coefficient of the $\sin(3\omega_{piezo} \cdot t)$ -term and a_2 the Fourier coefficient of the $\cos(2\omega_{piezo} \cdot t)$ -term. The scatterer generally produces phase changes much faster than the thermal phase drift, but much slower than the reference mirror/piezo stack oscillation. The OCM detects motion of individual scatterers by performing multiple consecutive x-scans (typically 6), and taking the difference between phases calculated for consecutive x-scans of the same voxel. Together with the time between successive visits to the same voxel, these phase differences yield the z-velocity of the scatterer. Our motion sensitive images display for each voxel the standard deviation of these five phase differences belonging to the same voxel, and are thus a measure of the jitter of the scatterer’s motion.

Fig. 4 shows two images of frog embryos during gastrulation, where the one on the left is taken with the 850 nm instrument, and the one on the right with the new 1300 nm OCM. The increased depth penetration of our 1300 nm OCM compared to that of the 850 nm OCM allows for a stronger signal in deeper tissue and therefore more reliable motion sigma values, as well as stronger contrast at the ectoderm-mesendoderm boundary.

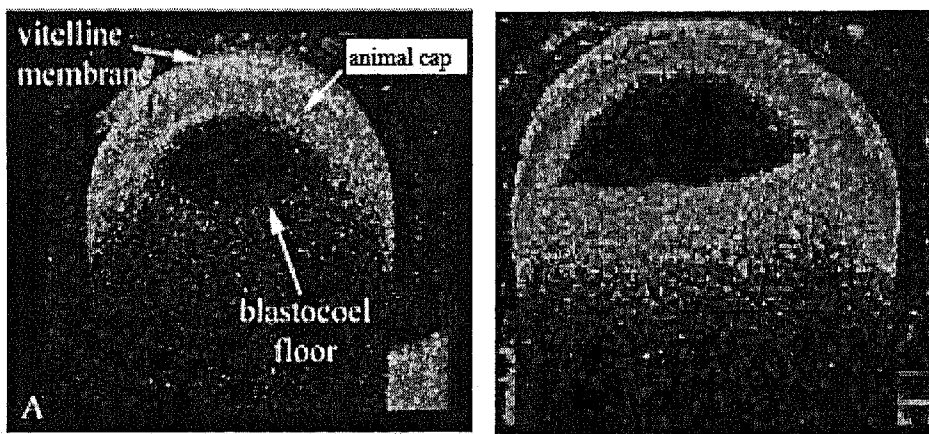


Fig. 4: Two motion-sensitive images of frog gastrulation. The one on the left is taken with the 850 nm OCM, the one on the right with the new 1300 nm instrument. Red voxels indicate strong diffusive motion, blue voxels minimal diffusive motion. [5]

3. RESULTS AND DISCUSSION

3.1 Frog Embryo Imaging

By inspecting the albino embryos under a light microscope we selected healthy ones for imaging, i.e. those that are spherically symmetric, of average size relative to the others (diameter ~ 1.2 - 1.4 mm), and among the more developed embryos of their batch, as measured by the number of visible cell divisions. *Xenopus laevis* embryos develop within a protective jelly coat surrounded by a thin sticky membrane that tends to cast shadows on the embryo in images. To avoid this shadowing, we mechanically removed the sticky membrane using two dissecting forceps under the light microscope. The embryos, now only surrounded by the protective jelly coating, were imaged in plastic Petri dishes filled with rearing buffer. They were simply placed on a stack of microscope slides (when imaged from above) or held lightly in place between an angled microscope slide and the Petri dish bottom (when imaged from below in a tilted Petri dish).

3.2 Interpretation of the frog embryo images

Fig. 5 below shows a fringe amplitude image of frog gastrulation at an early stage on the left, and a motion-sigma image on the right. Clearly, the motion-sigma image reveals information about the tissue that complements the features displayed in the fringe amplitude image. We observe a higher motion-sigma value in the vegetal (bottom) mass of the embryo which we attribute to the Brownian motion of yolk platelets in the vegetal yolk cells (endoderm). Yolk platelets, the cell organelles that contain the frog embryo's pre-stored nutrients, come in a wide range of sizes, mostly falling between $1\ \mu\text{m}$ to $10\ \mu\text{m}$ [6]. The larger, denser yolk platelets tend to settle in the most vegetal (bottom) region of the oocyte, while the lighter ones stay above. After fertilization, small yolk-free cells are found near the animal pole, and large yolk-filled cells in the vegetal hemisphere. When the embryo forms a blastula, the yolk-free cells make up the blastocoel roof while the large yolk-filled cells form the endoderm [7].



Fig. 5: 1300 nm OCM fringe amplitude image (left) and motion-sigma image (right) of early gastrulation. In the motion-sigma image, red voxels indicate strong diffusive motion, blue voxels minimal diffusive motion. Note the strong contrast between endodermal yolk cells (green/yellow) and ectodermal cells (blue). [5]

Figure 6 shows a time sequence of images taken during early gastrulation. All images are mid-sagittal sections with the dorsal side to the right and ventral side to the left.

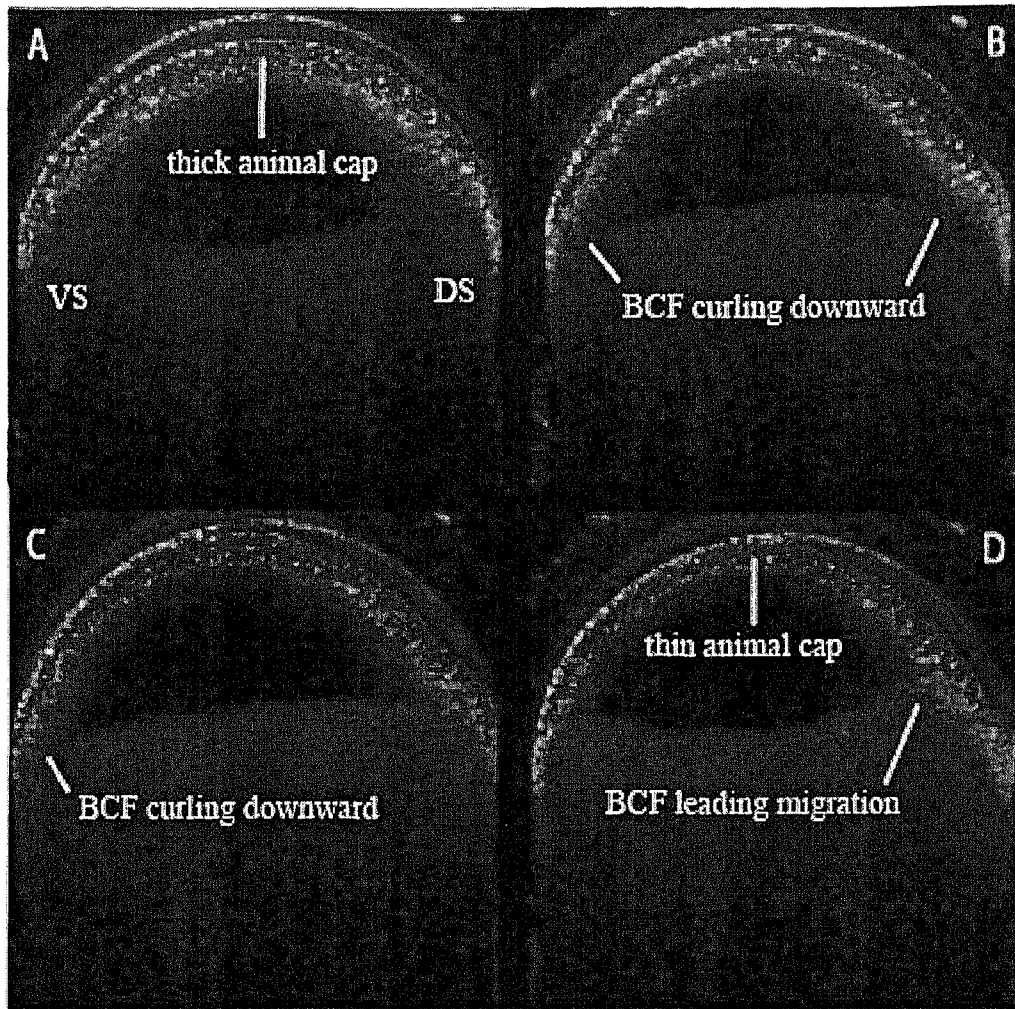


Fig 6: Images of the embryo undergoing vegetal rotation movements. The images are all mid-sagittal sections, i.e., cuts along the dorsal-ventral axis. The dorsal side (DS) is to the right, and the ventral side (VS) is to the left in all the images, although they are labeled only in (A). The embryos are approximately 1.5 mm in diameter. [5]

(A): 09 hrs 10 min. post fertilization (p.f.). The animal cap is still thick, and the blastocoel floor (BCF) has not expanded, so vegetal rotation has not begun.

(B): 11 hrs 40 min. p.f. The BCF has expanded considerably and the center of the BCF has moved upward. In addition, the peripheral edges of the BCF have curled downward indicating vegetal rotation is taking place.

(C): 12 hrs 11 min. p.f. The dorsal periphery of the BCF is not curled vegetally as much, but the ventral edge has curled vegetally slightly more. This suggests that vegetal rotation starts later on the ventral side, which was also observed by Winklbauer and Schürfeld.

(D): 13 hrs 25 min. p.f. The blastocoel floor is leading the mesendodermal migration up the BCF on the dorsal side to a greater extent than on the ventral side. The animal cap is visibly thinner in (D) as compared to (A).

Just prior to gastrulation, the embryo consists of a mass of undifferentiated cells with a fluid filled cavity in the upper half, called the blastocoel, as shown in Figure 6 A. The thin layer of cells above the blastocoel is the presumptive ectoderm, the mass of larger cells below the blastocoel is going to be the endoderm, and the cells between the future ectoderm and endoderm will be the mesoderm. Gastrulation is theorized to be initiated by a process called vegetal rotation in which the blastocoel floor expands and moves upward, while its peripheral edges are curling downward. It was first suggested by Winklbauer and Schürfeld on the basis of their studies of explant embryos that had their blastocoel roofs sliced off [8]. During gastrulation, the mesoderm and endoderm involute, or fold into, the embryo while the ectoderm spreads and thins to completely cover the embryo in a process called epiboly. The mesendoderm (mesoderm and endoderm) migrates up the inner surface of the ectoderm, ultimately displacing the blastocoel.

Our OCM instrument allows non-invasive imaging of opaque embryos *in vivo* and provides the temporal and spatial information of those live embryos or tissues to understand their development.

4. REFERENCES

- [1] B.E. Bouma and G.J. Tearney (editors), "Handbook of Optical Coherence Tomography", Marcel Dekker Inc. (2002).
- [2] B.M. Hoeling, A.D. Fernandez, R.C. Haskell, E. Huang, W.R. Meyers, D.C. Petersen, S.E. Ungersma, R. Wang, and M.E. Williams, "An optical coherence microscope for 3-dimensional imaging in developmental biology", *Optics Express* Vol.6, No.7, 136-146 (March 27, 2000).
- [3] B.M. Hoeling, A.D. Fernandez, R.C. Haskell, and D.C. Petersen, "Phase modulation at 100 kHz in a Michelson Interferometer using a piezoelectric stack driven at resonance", *Review of Scientific Instruments* Vol.72, 1630-1633 (2001).
- [4] B.M. Hoeling, M.E. Peter, D.C. Petersen, and R.C. Haskell, "Improved Phase Modulation for an *en-face* Scanning 3D Optical Coherence Microscope", *Review of Scientific Instruments* Vol.75, 3348 (2004).
- [5] To view the images in color, please go to:
<http://www.physics.hmc.edu/research/ocm/>
- [6] S. Komazaki et al., "Regional differences in yolk platelet degradation activity and in types of yolk platelets degraded during early amphibian embryogenesis." *Cells Tissues Organs*. 172: 13-20 (2002).
- [7] J. Hardin, "Cleavage of Mesolecithal Eggs: Amphibians." (updated Jan. 16, 2006). *Developmental Biology Online* (2002).
- [8] R. Winklbauer and M. Schürfeld, "Vegetal rotation, a new gastrulation movement involved in the internalization of the mesoderm and endoderm in *Xenopus*." *Development* 126: 3703-3713 (1999).